Macromolecules

pubs.acs.org/Macromolecules Article

Photo-Controlled Dynamics and Transport in Entangled Wormlike Micellar Nanocomposites Studied by XPCS

Mario Reiser,* Jörg Hallmann, Johannes Möller, Karina Kazarian, Davide Orsi, Lisa Randolph, Hendrik Rahmann, Fabian Westermeier, Eric Stellamanns, Michael Sprung, Federico Zontone, Luigi Cristofolini, Christian Gutt, and Anders Madsen*

Cite This: *Macromolecules* 2022, 55, 8757–8765 Read Online

ACCESS | Metrics & More | Article Recommendations | Supporting Information

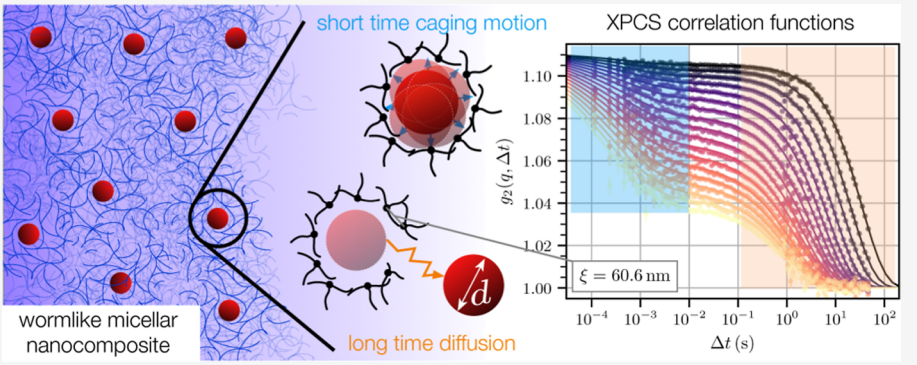

ABSTRACT: Dynamics of nanoparticles (NPs) in microscopic networks, in particular, localization and transport, play a key role in designing new functional nanocomposites and drug delivery systems. To this aim, it is crucial to understand the interplay between the network structure and dynamics on the microscopic scale which determines NP diffusion. Here, we study the localization and transport of spherical NPs in photorheological wormlike micellar nanocomposites where the mobility of the NPs is controlled by the network mesh size and the micelle length, which can be tuned by UV-illumination. The macroscopic viscoelastic properties are measured by classical rheology, while X-ray photon correlation spectroscopy and nanorheology provide information on the microscopic NP dynamics on length scales on the order of the network mesh size. On long time scales, the data reveal that transport through the network is determined by the ratio between the NP size and the network mesh size, while upon UV illumination, the NP mobility is drastically enhanced. On shorter time scales, the influence of the dynamical and structural micelle properties on the NP dynamics under confinement is explored and indicates an anomalous speed-up of the dynamics, which is discussed in the context of changes in the local structure and non-linear phenomena such as strain stiffening and hopping motion.

INTRODUCTION

The dynamics of nanoparticles (NPs) in microscopic networks and other crowded environments are of interest in a broad range of fields from physics, chemistry, and biology to engineering and material science. On a macroscopic length scale, the presence of NPs can alter the magnetic,[1] optical,[2,3] viscoelastic, or mechanical[4,5] properties of the system. On a microscopic length scale, the NPs are trapped inside network cages where localization and diffusion through the medium[6−9] are relevant for instance for drug delivery and information transport,[10] for example, by controlling the release mechanism. In this context, two main aspects are important: first, the effect of the network structure and dynamics on the localization of the NPs; second, the characteristic dynamics of the localized NPs and which processes contribute to confinement release. For instance, it has been a longstanding discussion to which extent activated hopping[6,11] plays a role for NP motion. Being able to capture both localized cage dynamics and long-time diffusion simultaneously will open new pathways to explore localization and transport in complex networks. A detailed characterization of the dynamics is also crucial for diverse nanorheology techniques where the local viscoelastic properties of a specimen are deduced from the dynamics of tracer particles.[12−14]

Flexible microscopic networks usually consist of long cylindrical or wormlike molecules that form an entangled or cross-linked network. Polymers and micelles are two

Received: June 27, 2022
Revised: September 2, 2022
Published: September 26, 2022

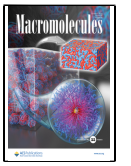

prominent examples. While polymers consist of covalently bonded monomers, micelles are aggregates of surfactant molecules that self-assemble to form various types of structures when the surfactant concentration exceeds a critical value. The micellar shape is determined by properties of the surfactant molecule, in particular, by the ratio of the volumes of its hydrophobic and hydrophilic parts. Wormlike micelles are formed when the surfactant molecules self-assemble and attain cylindrical shape.[15,16] Micelles are promising candidates in the pursuit of new "smart" materials that change their function and structure in response to external stimuli (electrical, optical, thermal, etc.).[17−19] In contrast to covalently bonded polymer networks such as hydrogels, micelles are transient structures which undergo random scission and recombination that affect the stress relaxation on long time scales.[20] However, on short time scales these processes are negligible and the micelles are stable. Analogously to polymer networks, the microscopic micelle network is described by a hydrodynamic correlation length or network mesh size, ξ, which is a measure of the average distance between entanglement or branching points.[15] Localization and NP dynamics in the network are highly depending on the network structure, in particular the ratio between ξ and the NP size, d.[9]

Experimentally, it is challenging to investigate dynamics in microscopic networks on length scales comparable to the cage size and below, especially in concentrated solutions. In fact, most experimental studies focus on the slower structural network relaxation due to technical limitations, in particular lack of temporal resolution.[14,21] The localized motion inside a cage can be several orders of magnitude faster than the structural relaxation. By X-ray photon correlation spectroscopy (XPCS),[22−25] it is possible to study sub-millisecond dynamics and, thereby, gain insight into localization of NPs in microscopic networks and other dynamical phenomena in complex fluids. XPCS obtains dynamical information from speckle intensity fluctuations—an interference phenomenon visible in the far field when the sample is illuminated by (partially) coherent light (Figure 2). This allows investigation of length scale-dependent dynamics of the NPs on the microscopic scale due to the short X-ray wavelength. Novel X-ray detectors are capable of acquiring scattering images with several kilohertz repetition rate so that a wide range of time scales from microseconds to hundreds of seconds can be investigated (Figure 3).

Ketner et al.[26] found that the mechanical response of wormlike micelle suspensions formed by cetyl trimethylammonium bromide (CTAB)[15,27] and *ortho*-methoxycinnamic acid (OMCA)[28,29] can be tuned by UV illumination. UV illumination causes isomerization of the OMCA molecules that desorb from the micelle surface and reduce the end-cap energy. As a result, the average micelle contour length decreases. Although wormlike micelles can be described as flexible chains, they exhibit short-range rigidity described by the Kuhn-length, b.[30] Figure 2 illustrates that a flexible micelle can be approximated by a chain of rigid cylinders with length, b.

Here, the viscoelastic properties of the OMCA−CTAB system and the influence of UV illumination is studied by classical rheometry on a macroscopic level. Deeper insights into the local viscoelastic properties of the micelle network are obtained from XPCS nanorheology measurements, which further provide information on the NP mobility and transport through the micelle network. The results show how the transport properties of the NPs can be tuned by varying the network mesh size and UV illumination. On sub-millisecond time scales, the motion of the NPs under confinement inside the network meshes is studied by XPCS. The results evidence how the network mesh size determines the confinement properties of the cage. While the mesh size determines the NP confinement, UV illumination speeds up the NP motion by shortening the average micelle length which is seen in the ergodicity restoring part of the XPCS correlation functions.

SAMPLE PREPARATION

OMCA−CTAB samples were synthesized according to the recipe of Ketner et al.[26] The OMCA concentration was equal to the CTAB concentration for all solutions. Aqueous solutions of OMCA and CTAB were prepared and spherical silica NPs (d = 100(4) nm) were dispersed in the CTAB solution to ensure a homogeneous distribution in the highly viscous network. The NP volume fraction (0.04%) was kept as low as possible to still provide a scattering signal for the XPCS measurements. Rheology measurements indicate that the effect of the NPs on the viscoelastic network properties, and hence on the micelle formation, is negligible (see Supporting Information). 15 min after mixing both solutions and stirring, the samples were filled into quartz capillaries with an outer diameter of 2 mm for the XPCS measurements.

The absorbed energy when illuminating the sample with UV light is calculated as $E_{UV} = I_{UV}A_{UV}t_{UV}$, where I_{UV} is the intensity of the UV light and t_{UV} is the illumination time. The absorption of a solution with concentration c and sample thickness d_s is defined as $A_{UV}(c, d_s) = (1 - e^{-\log(10)\varepsilon d_s c})$, where ε is the molar extinction coefficient. ε = 0.0164 mM^{-1} is estimated at the position of the main absorption peak of *trans*-OMCA at λ = 270 nm.[26] I_{UV} was measured with a power meter.

RHEOLOGY MEASUREMENTS

Rheology measurements were conducted with a HAAKE MARS III rheometer at the Deutsches Elektronen-Synchrotron (DESY). By fitting the complex moduli with a Maxwell model, the plateau modulus, G_0, the terminal time, τ_R, and the viscosity, η, were determined (see the Supporting Information for more details), where $\eta = \tau_R G_0$. Figure 1 displays G_0, τ_R, and η as a function of concentration (a) and UV illumination (b). The concentration was varied from 20 to 200 mM. Figure 1a shows that the concentration dependency of the viscosity can be described by a power law ($\eta(c) \propto c^{m_\eta}$) with an exponent of m_η = 2.2(3). This exponent is smaller than predicted within the reptation model by scaling theory (m_η = 3.7) and mean-field theory (m_η = 3.5),[31] which can be explained by the essentially concentration-independent terminal time as indicated by the horizontal dashed line. The anomalous concentration dependence of the viscosity can be attributed to intermicellar branching. Micelle branching occurs when an entanglement is replaced by a joint between adjacent micelle strands resulting in a cross-link.[32,33] As joints are prone to slide along the micelle contour, they are effectively "softer" than entanglements and hence weaken the concentration dependence.[34]

The effect of UV illumination on the rheological properties on a 80 mM micelle solution is shown in Figure 1b. The upper, fixed plate of the rheometer was exchanged with a quartz plate such that the sample could be illuminated inside the rheometer. The UV light intensity was measured with a

https://doi.org/10.1021/acs.macromol.2c01326
Macromolecules 2022, 55, 8757−8765

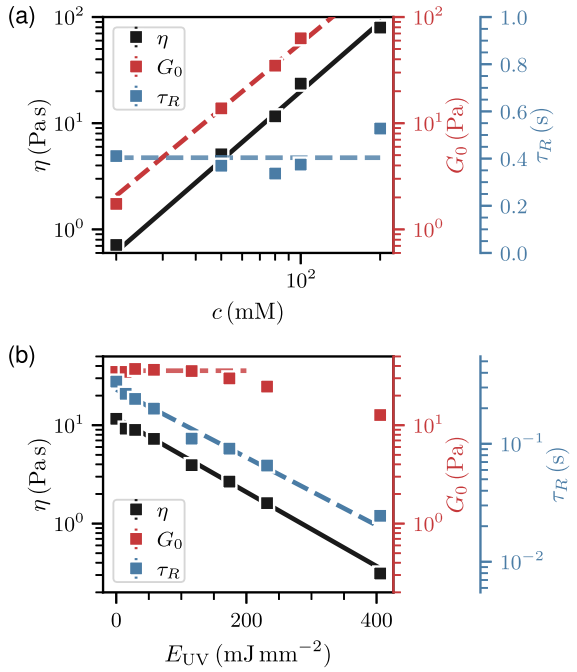

Figure 1. Rheology experiments performed with a plate−plate rheometer: dynamic viscosity, η, plateau modulus, G_0, and terminal time, τ_R, as a function of micelle concentration in (a) and as a function of UV-illumination for an 80 mM solution (b). $\eta(c)$ is fitted with a power law with an exponent of $m_\eta = 2.2(3)$ (solid black line). The dashed lines are guides to the eye. In (b), an exponential decay is used to model the decreasing viscosity and a decay constant of (115 ± 3) mJ mm^{-2} is determined by the fit (solid black line). The dashed lines are guides to the eye.

power meter at the sample position, that is, below the quartz plate of the rheometer. The viscosity in Figure 1 decreases exponentially with UV illumination with a decay constant of (115 ± 3) mJ mm^{-2}. In contrast to varying the concentration, the data imply that the UV illumination dependence of the viscosity is solely determined by the terminal time. While τ_R is strongly affected by UV illumination, G_0 is constant within the measurement accuracy for $E_{UV} \lesssim 200$ mJ mm^{-2} and starts to decrease only for longer UV illuminations. The decreasing viscosity as a function of UV illumination can be explained by the formation of new end-caps accompanied by the breaking of cross-links or the scission of micelles, which effectively reduces the connectivity of the branched micelle network.

In summary, Figure 1 shows that the viscosity can be tuned by changing concentration or UV illumination. However, the origin of the viscosity change is different. Varying the micelle concentration affects the plateau modulus which is related to the network mesh size while the terminal time is constant. In other words, the concentration determines the network connectivity but its effect on the network relaxation time is negligible. On the other hand, the terminal relaxation time decreases as a result of the UV induced shortening of the micelles, while the network mesh size is constant for short UV illumination times. Hence, the network relaxation can be tuned by UV illumination, while the network structure remains unaffected.

XPCS DATA TREATMENT

XPCS experiments were conducted at P10 at PETRA III (DESY) and ID10 (ESRF) employing (partially) coherent X-rays with a photon energy of 8.1 keV. A Si(111) monochromator reduced the bandwidth to $\Delta E/E \approx 10^{-4}$ to increase the longitudinal coherence. The experiments at ID10 were conducted with a beam size of 10 μm and a sample-detector distance of 5.1 m. At P10, the beam size was increased to 75 μm to obtain a lower radiation dose. Consequently, the sample-detector distance must be increased to have an adequate speckle contrast and 21.2 m was used. Figure 2

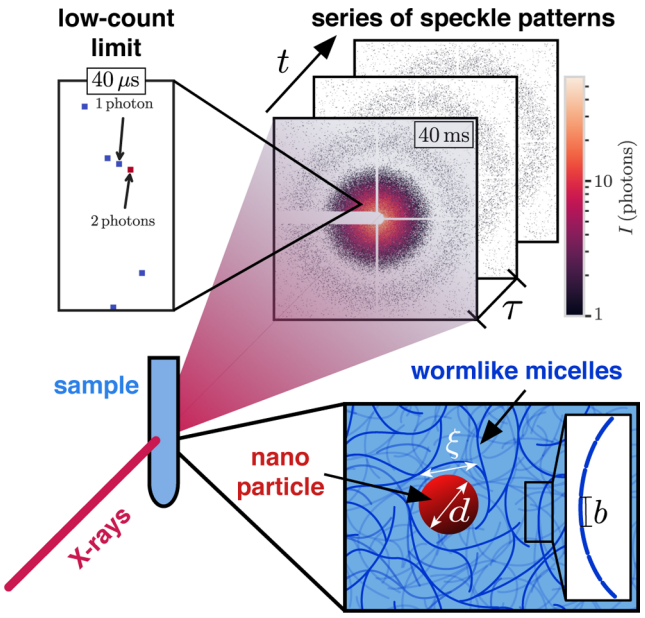

Figure 2. Experimental schematics: NPs (d = 100 nm) are dispersed in OMCA−CTAB micelle solutions. ξ is the mesh size of the network and b the Kuhn-length. The micelle contour length can reach several hundred nanometers.[26] The sample is illuminated by (partially) coherent X-rays and series of speckle patterns are acquired by a 2D detector with different exposure times (indicated on the images) down to the limit of only a few photons registered per frame.

shows the schematic experimental layout. The OMCA−CTAB solutions were measured in quartz capillaries with a diameter of 2 mm which also allowed illuminating the solutions inside the capillaries by UV light.

The X-ray scattering contrast of the silica particles is orders of magnitude larger than the one of the OMCA−CTAB micelles so that the measured speckle fluctuations can be attributed solely to the NP dynamics. Two-time correlation functions[25] were employed to identify the onset of radiation damage yielding a dose threshold of 2 kGy which corresponds to less than 1 s illumination by the unattenuated beam (see the Supporting Information). Consequently, data were acquired until this threshold was reached. Afterwards, the beam position on the sample was changed for the next measurement leading to hundreds of acquired time series per sample. Attenuating the beam allowed longer acquisitions and studying longer time scales. Thereby, the correlation functions could be measured step-wise and stitched together covering a time window from microseconds to tens of seconds (Figure 3). This procedure yields one set of correlation functions (different q-values) per sample (one capillary of OMCA−CTAB solution). Several capillaries with solutions of a given concentration were measured and treated separately to avoid averaging over slightly different sample conditions for instance due to aging. Therefore, during the discussion, the solutions will be

https://doi.org/10.1021/acs.macromol.2c01326
Macromolecules 2022, 55, 8757−8765

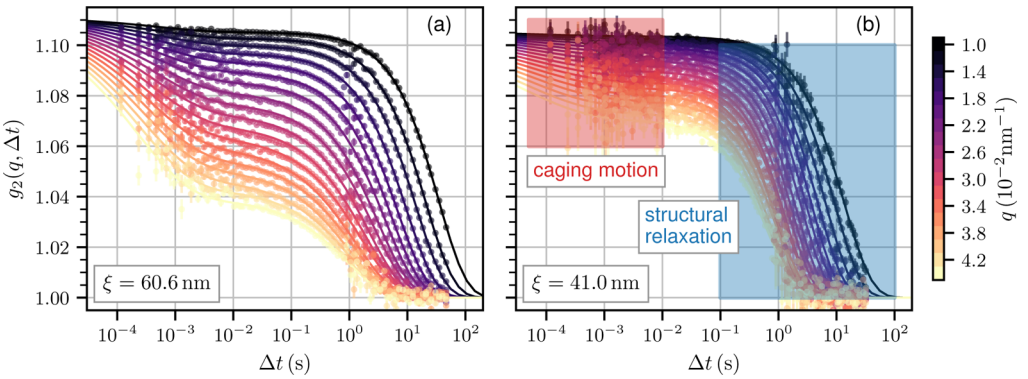

Figure 3. Intensity auto-correlation functions, $g_2(q, \Delta t)$, of 100 nm silica NPs dispersed in OMCA−CTAB solutions of 50 mM (a) and 80 mM (b) surfactant concentration. The two relaxation modes are indicated in blue and red in panel (b). Solid lines are fits with eq 1.

characterized by their mesh size determined from the correlation functions rather than from the initial concentration.

The correlation functions in Figure 3 exhibit a two-step relaxation indicative of structural network dynamics on long time scales and caging motion of localized NPs on short time scales. Hence, the correlation functions can be modeled by the sum of two exponential modes

$$g_2(q, \Delta t) = 1 + \beta_0 \sum_{i=1}^{2} \beta_i(q) \exp\{-2(\Gamma_i(q)\Delta t)^{\alpha_i(q)}\} \quad (1)$$

where Γ_i are the relaxation rates and α_i are Kohlrausch−Williams−Watts (KWW) exponents. The indices 1 and 2 are referring to the short- and long-time relaxations, respectively (Figure 3). β_0 is the maximum speckle contrast, that is, the contrast of a static sample, and β_i are the relative strengths with $\beta_1 = 1 - \beta_2$. The contrast of the plateau that separates both processes, β_2, is also denoted the non-ergodicity level.

The non-ergodicity level is decreasing as a function of q which is usually modeled by a Debye-Waller-like function: $\beta_2 = \exp(-r_{\mathrm{loc}}^2 q^2/3)$.[24] The localization length, r_{loc}^2, is the mean-squared displacement of the NPs under confinement and is related to the mesh size ξ by[9]

$$\xi^3 = r_{\mathrm{loc}}^2 d = k_B T / G_0 \quad (2)$$

Equation 2 allows comparing XPCS and classical rheology where ξ is inferred from the measured plateau modulus G_0. The resulting ξ values calculated from rheology using eq 2 are displayed in Figure 4 (gray squares) as a function of concentration, c. The measurements were repeated up to five times per concentration. The standard deviations $\Delta\xi$ are indicated by the error bars. However, the error of an individual XPCS measurement determined from the fit is $\delta\xi \lesssim 2$ nm. The characteristic network length scales determined by both methods (XPCS and rheology) are in agreement underlining the validity of the approach. A power law fit (Figure 4, solid line) results in a scaling exponent of −0.72(6) as expected for a network of semi-flexible wormlike micelles.[35]

Information about the underlying dynamics is encoded in the dispersion relations, $\Gamma_i(q)$. Figure 5 (left panels) displays

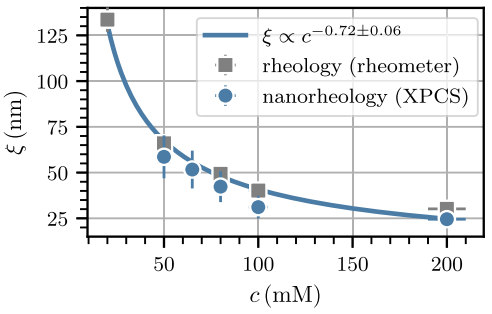

Figure 4. Hydrodynamic correlation length, ξ, determined by XPCS based nanorheology and classical rheology with a plate−plate rheometer (see eq 2). $c = c(\mathrm{OMCA}) = c(\mathrm{CTAB})$ is the concentration of both OMCA and CTAB. The solid line indicates a power law fit.

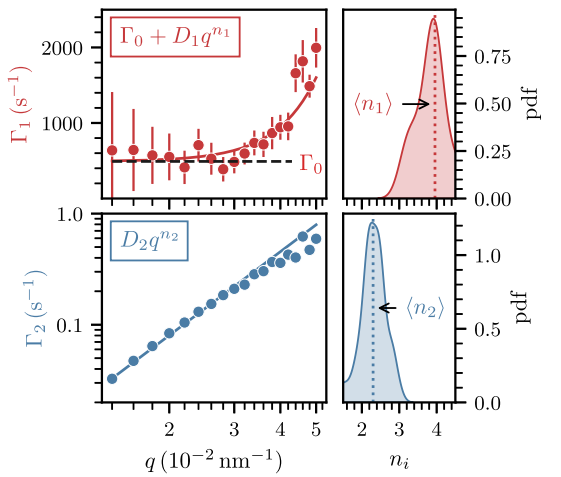

Figure 5. (Left panels) Dispersion relations of the localized caging motion and the structural network relaxation are plotted in red and blue for one set of correlation functions: the 50 mM micelle solution from Figure 3a. The functional forms of the dispersion relations used to fit the data (solid lines) are indicated in the panels. (Right panels) Distributions of the exponents, n_i, of all samples (in total 25). The average values $\langle n_i \rangle$ are annotated.

the relaxation rates obtained from the data in Figure 3a for a micelle solution of 50 mM. The slow structural relaxation (blue) is well modeled by a power law of the form $\Gamma_2(q) = D_2 q^{n_2}$, whereas the short-time dispersion relation, $\Gamma_1(q)$ (red), can be described by a power law plus a constant plateau[36]

$$\Gamma_1(q) = D_1 q^{n_1} + \Gamma_0 \quad (3)$$

D_i are generalized diffusion coefficients and n_i are the corresponding scaling exponents of both relaxation processes. While D_i measure the amplitude of the dynamics, n_i indicate

https://doi.org/10.1021/acs.macromol.2c01326
Macromolecules 2022, 55, 8757−8765

the type of dynamics; for instance, Brownian motion would yield $n = 2$.

Interestingly, $\Gamma_1(q)$ exhibits a plateau ($\Gamma_0 > 0$) for small momentum transfers which is characteristic of confined dynamics. While $\Gamma_2 = Dq^2$ holds for diffusion in an infinite medium, the presence of finite cages results in a constant contribution to the dispersion relation in case of localized dynamics, that is, the fast relaxation process. This phenomenon has previously been observed for instance in fullerides by quasielastic neutron scattering.[37,38] With microsecond XPCS, it is possible to study these localization effects in the time domain. In addition, $q_0 = \sqrt[n_1]{\Gamma_0/D_1}$ is the momentum transfer where the cross-over from a power law behavior to the constant plateau occurs. Then, the dynamical cage size is approximately given by $L_0 = 2\pi/q_0$.

Correlation functions of different q-bins are fitted with eqs 1−3 to determine the dynamical parameters. The reader is referred to the Supporting Information for a detailed description of the data treatment. Figure 5 (right panels) displays histograms of the q-scaling exponents, n_i, over the acquired data sets yielding one pair (n_1, n_2) per sample. The mean values of the corresponding distributions, $\langle n_i \rangle$, reflect the different nature of the two relaxation processes. While the structural relaxation (blue) exhibits close to diffusive behavior ($\langle n_2 \rangle = 2.3$), the short-time caging motion is found to be subdiffusive with $\langle n_1 \rangle = 4$. Subdiffusivity originates from restricted motion of NPs inside network cages and is hence another evidence for confinement. The KWW exponents, α_1 (not shown), support the same picture with $\alpha_1 \approx 0.5$, that is, the correlation functions resemble stretched exponential behavior corresponding to the mean-squared displacement increasing proportional to $\sqrt{t}$ at short times.

SHORT-TIME DIFFUSION AND CAGING MOTION

XPCS allows us to study the NP dynamics under confinement, that is, before a NP leaves a network cage. When a NP is trapped inside a network cage, its short-time dynamics are strongly determined by the properties of the confining cage described by the microscopic parameters Γ_0, L_0, and ξ. While ξ is an intrinsic network property, Γ_0 and L_0 depend on the NP size. Both parameters are only defined if the NPs are localized. There are two extreme cases where localization cannot be observed: if $\xi \gg d$, the NP dynamics are not influenced by the network and can basically diffuse unhindered in the solution. On the other hand, if $\xi \ll d$, the NPs are much larger than the network mesh and the surrounding micelles can be approximated as a homogeneous medium on length scales of the NP size.

To investigate the influence of the network mesh size on the localization of the NPs, the experimentally determined values of Γ_0 and L_0 are plotted as functions of ξ in Figure 6. Localization effects are pronounced in a ξ-range from 30 to 65 nm for 100 nm particles. Within this range the particles are trapped in network cages on short-time scales. L_0 shows a minimum at ∼46 nm which is a bit smaller than the NP radius (Figure 6a). We denote this situation *ideal confinement* as the NPs are localized within network cages with the minimum possible volume. Caging effects lead to a value of Γ_0 larger than zero (Figure 6b). The behavior of Γ_0 can be modeled by a quadratic function (black dashed line) with a maximum at roughly the same position as the minimum of L_0 emphasizing the connection between the parameters.

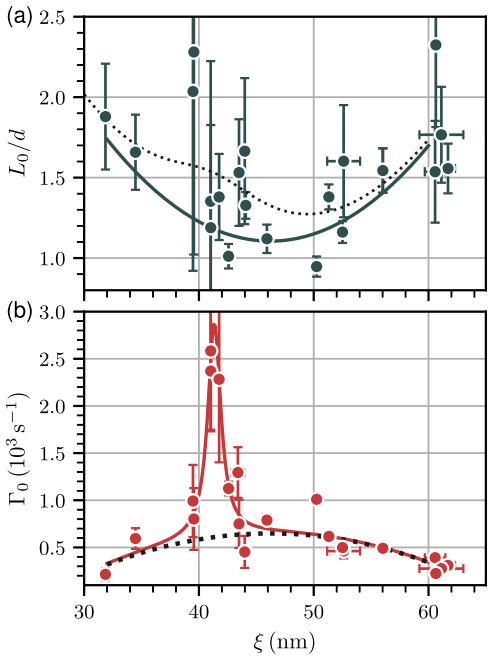

Figure 6. (a) Dynamical cage size, L_0, in units of the particle size, d. A quadratic model (solid line) is used to describe the data. The dashed line serves as a guide to the eye and emphasizes the situation where higher weights are given to the data with high uncertainty around $\xi \approx$ 42 nm. (b) Γ_0 plotted versus the mesh size, ξ. The data are modeled by a Lorentzian function plus a quadratic background (red solid line). The peak position is $\xi_0 = 41.2(2)$ nm. The quadratic background is plotted as a dashed black line.

Surprisingly, Γ_0 exhibits a peak [FWHM 2.1(5) nm] where its value increases by a factor of four compared to the quadratic background. The peak position, $\xi_0 = 41.2(2)$ nm, is shifted toward smaller mesh sizes with respect to the maximum of the quadratic background. The rapid increase of Γ_0 points toward an enhanced NP mobility in a short range of mesh sizes indicating that additional processes drive the NP dynamics. The dashed line in Figure 6a emphasizes that the values found for L_0 exhibit an anomalous increase in the same range of mesh sizes. The large error bars stem from the uncertainty of the parameters n_1 and D_1 which are used to determine L_0 in addition to Γ_0. The data analysis methods are explained in detail in the Supporting Information showing that the calculation of Γ_0 is uncorrelated to the other fit parameters. Conclusively, the peak of Γ_0 is not related to the uncertainty in the calculation of L_0 but is a result of the NP dynamics.

The observed enhancement of NP mobility is related to the local cage structure and dynamics of adjacent network strands; however, the exact mechanism remains elusive. The strong increase of the NP dynamics by about a factor of four allows speculation about contributions from different processes. The local cage structure is determined by the network interconnections that, in case of the transient OMCA−CTAB micelle network, differ from permanent cross-links of polymer networks or melts. For instance, micelles can form branching points that are prone to slide along the micelle contour which effectively results in "softer" network connections compared to entanglements and cross-links.[32,33,39] Intermicellar branching could affect the NP dynamics by changing the confinement conditions. It could also be envisioned that chain-end fluctuations contribute to the NP dynamics in confinement in a similar fashion.

https://doi.org/10.1021/acs.macromol.2c01326
Macromolecules 2022, 55, 8757−8765

Thermally activated barrier hopping has been proposed as a mechanism that affects NP dynamics. It describes the spontaneous transition of a NP from one network cage to the next one through a randomly enlarged network mesh. Hopping occurs on faster time scales than reptation-driven confinement release and is predicted only for a small ξ-range of $d/2$ to $2d/3$ ($\approx$50 to 67 nm).[6,11] The peak position in Figure 6b does not fall precisely into the predicted window for hopping but is shifted toward smaller mesh sizes. Similar to activated hopping, the enhanced NP mobility could be explained as an activated process that is only observed in a particular network configuration.

The length scale corresponding to the peak position in Figure 6b is comparable to the Kuhn-length, b (see Figure 2), found for wormlike CTAB micelles[30] and, therefore, might indicate a connection between short-range rigidity of the micelles and localized cage dynamics of the NPs. Confined NP diffusion might lead to the deformation of micelle strands which below the Kuhn-length can show a non-linear mechanical response similar to strain-stiffening.[40−43] Experimentally, these phenomena are usually studied with conventional rheology techniques and in model systems such as collagen fibers with macroscopic Kuhn-lengths (~1 cm)[44] but usually signatures of these effects on microscopic networks are difficult to obtain in such experiments due to the limited spatial resolution.

LONG-TIME DIFFUSION AND TRANSPORT

The long-time diffusion of the NPs is discussed in the context of the classical rheometry results described previously. Figure 7

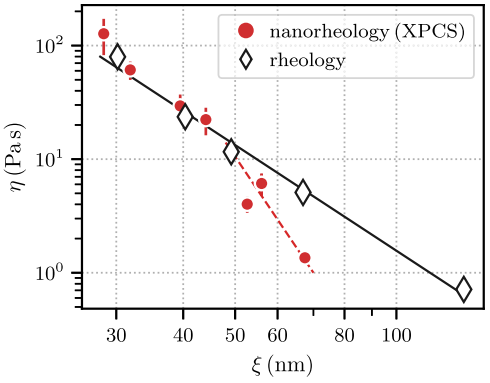

Figure 7. Dynamic viscosity, η, as a function of mesh size, ξ. The diamonds show the rheology measurements performed with a plate−plate rheometer and the circles show the viscosity obtained from XPCS nanorheology measurements employing the Stokes−Einstein relation. The solid black line indicates a power law fit with an exponent of 3.53(13). The dashed red line indicates the deviation of the XPCS data from the rheology data.

displays the viscosity of several OMCA−CTAB solutions measured with rheometry (diamonds) and calculated with nanorheology employing the Stokes−Einstein relation $\eta = k_B T/(6\pi R_h D_2)$, where k_B is the Boltzmann constant, T is the temperature, and R_h is the hydrodynamic radius. The data are plotted against the network mesh size ξ. The black line depicts a power law model of the rheometer data with an exponent of 3.53(13). For a mesh size above 50 nm, the results indicate that the XPCS nanorheology data start to deviate from the macroscopic viscosity emphasized by the red dashed line. In particular, the viscosity experienced by the NPs is smaller than the macroscopic viscosity, hence indicating faster dynamics. As the mesh size becomes larger, the NPs are able to slip through network meshes and therefore experience a lower local viscosity. This effect is crucial for the NP mobility and microscopic transport properties as the network mesh size needs to be small enough to actually provide confinement for the NPs.

The data further indicate that the onset of deviation from the Stokes−Einstein prediction occurs for $\xi > 50$ nm, which is the NP radius. Intuitively, one would expect the mesh size threshold to be close to the particle size $d = 2R$. NP dynamics in polymer melts have been hypothesized to exhibit an intermediate regime from $\xi \approx 2R$ to $\xi \approx R$, where Stokes−Einstein behavior is gradually recovered.[8] Although the range of investigated mesh sizes is insufficient to really evaluate how well the model in ref 8 applies to the OMCA−CTAB system, Figure 7 shows that the microscopic viscosity experienced by the NPs deviates from the macroscopic viscosity if the NPs are not trapped inside the network.

Figure 8 displays the diffusion coefficients D_2 as a function of UV illumination for three different initial micelle concen-

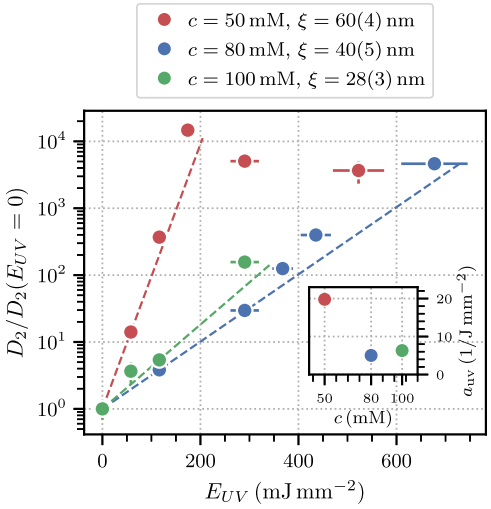

Figure 8. NP diffusion coefficients, D_2, as a function of UV illumination normalized to the diffusion coefficients of the unilluminated sample. The dashed lines are guides to the eye. The color indicates the micelle concentration and the corresponding mesh size. The dashed lines show an exponential fit $y = 10^{E_{UV}/a_{uv}}$. a_{uv} is the rate at which the diffusion coefficients are increasing per unit UV fluence.

trations. The data are normalized to the unilluminated diffusion coefficient $D_2(E_{UV} = 0)$ to emphasize the effect of the UV illumination and exclude effects due to different initial viscosities. The legend also indicates the average mesh size of all the solutions of one concentration, where the error is the standard deviation over samples with the same micelle concentration, including all UV illuminations. The negligible UV illumination dependence of ξ indicated by the standard error in the legend is in line with the rheometry results displayed in Figure 1b. The increase of the diffusion coefficient with UV illumination can be explained by the decrease in viscosity as a result of the shorter micelle contour length. The 50 mM data indicate that after long enough UV illumination a plateau is reached where D_2 has increased by almost 4 orders of magnitude.

https://doi.org/10.1021/acs.macromol.2c01326
Macromolecules 2022, 55, 8757−8765

Strikingly, the dynamics of the NPs in the 50 mM solution increase about a factor of 3 faster compared to the 80 mM and the 100 mM solution. The inset displays the increase rate of D_2 with UV illumination modeled by an exponential. The fits are plotted as dashed lines in the main panel. The increased susceptibility to UV illumination of the NP dynamics in the 50 mM micelle solution can be attributed to the decreased NP localization due to the comparably large network mesh size. As discussed in Figure 7, if the network mesh size exceeds the NP radius, the dynamics differ from the Stokes−Einstein predictions based on the macroscopic viscosity. This is the case for the 50 mM solutions where the mesh size is about 60 nm. Interestingly, this deviation increases with UV illumination and does not disappear after scaling the data by $D_2(E_{UV} = 0)$; therefore, it cannot solely be explained by the decrease in solution viscosity. The NP dynamics are affected by the local micelle structure and cannot be deduced from macroscopic measurements, which is also illustrated by Figure 7. Therefore, methods such as XPCS are clearly required to provide direct access to the dynamic properties of crowded media on microscopic length scales. UV illumination reduces the average micelle length by decreasing the end-cap energy.[26] We hypothesize that, as the network mesh size increases, the NPs are gradually released from confinement and their dynamics start to be influenced by individual micelle strands rather than the network viscosity. Accompanied by the reduction in average micelle length is the creation of new micelle end-caps such that chain-end effects could influence the NP dynamics. In this picture, the UV-induced change of the average micelle structure affects the NP dynamics stronger in the loosely confined state, that is, here, the 50 mM solution.

These results underline that the dynamics of NPs in microscopic networks can significantly differ from predictions based on macroscopic measurements, thus rendering the development of experimental techniques such as XPCS, which allow to study the NP dynamics directly, important for understanding the microscopic processes of confinement and release.

CONCLUSIONS

In order to understand short-time processes on microscopic length scale in complex networks and to design new functional nanocomposites, the coupling of structural and dynamical network properties has to be studied locally. In this work, localization and transport were investigated by XPCS nanorheology providing unique dynamical information on the micelle network and dynamics of the NP probes. To access the relevant quantitative parameters, XPCS correlation functions were measured as a function of q over a wide range of timescales, here almost 6 orders of magnitude.

On short time scales, the NP dynamics under confinement were investigated and characterized by calculating the dynamical cage size and the plateau in the short-time dispersion relation. It was observed how the structural and dynamical cage properties change as a function of the network mesh size where the smallest cage size is found for a network mesh size slightly smaller than the NP radius. Surprisingly, over a narrow range of mesh sizes, the NP motion speeds up significantly by an increase in the short-time dispersion plateau, hence reflecting changes in the local cage structure. The enhanced NP dynamics are discussed in the context of different possible contributions such as chain-end fluctuations, activated hopping, and microscopic rigidity.

On long time scales, the dynamics of NPs in entangled and branched micelle networks have been studied by varying the network mesh size and the average micelle length by UV illumination and by changing the concentration. The XPCS nanorheology data were compared with classical rheometry and the results show that if the network mesh size exceeds the NP radius, the dynamics is faster than the Stokes−Einstein prediction using the macroscopic viscosity, hence indicating that NPs escape confinement by slipping through the network meshes.

UV illumination reduces the average micelle length and consequently the sample viscosity. The NP dynamics exhibit a particularly strong susceptibility to the reduction of the micelle length in case of weak confinement, that is, when the network mesh size is larger than the NP radius. We hypothesize that the strong increase of the NP dynamics in this case is related to an enhanced coupling of the NP dynamics to free micelle motion instead of the network relaxation.

We believe the presented experiments and results underline the need for local dynamical information in addition to classical rheology and pave the road for future investigations of dynamics in complex microscopic networks using XPCS.

ASSOCIATED CONTENT

Supporting Information

The Supporting Information is available free of charge at https://pubs.acs.org/doi/10.1021/acs.macromol.2c01326.

Rheology experiments, XPCS measurement protocol, and data treatment (PDF)

AUTHOR INFORMATION

Corresponding Authors

Mario Reiser − *European X-Ray Free-Electron Laser Facility, 22869 Schenefeld, Germany; Department Physik, Universität Siegen, 57072 Siegen, Germany;* orcid.org/0000-0003-0160-9478; Email: mario.reiser@xfel.eu

Anders Madsen − *European X-Ray Free-Electron Laser Facility, 22869 Schenefeld, Germany;* Email: anders.madsen@xfel.eu

Authors

Jörg Hallmann − *European X-Ray Free-Electron Laser Facility, 22869 Schenefeld, Germany*

Johannes Möller − *European X-Ray Free-Electron Laser Facility, 22869 Schenefeld, Germany;* orcid.org/0000-0001-8363-9077

Karina Kazarian − *European X-Ray Free-Electron Laser Facility, 22869 Schenefeld, Germany*

Davide Orsi − *Department of Mathematical, Physical and Computer Sciences, University of Parma, 43124 Parma, Italy;* orcid.org/0000-0003-3223-8622

Lisa Randolph − *Department Physik, Universität Siegen, 57072 Siegen, Germany*

Hendrik Rahmann − *Department Physik, Universität Siegen, 57072 Siegen, Germany*

Fabian Westermeier − *Deutsches Elektronen-Synchrotron, 22607 Hamburg, Germany*

Eric Stellamanns − *Deutsches Elektronen-Synchrotron, 22607 Hamburg, Germany*

Michael Sprung − *Deutsches Elektronen-Synchrotron, 22607 Hamburg, Germany*

https://doi.org/10.1021/acs.macromol.2c01326
Macromolecules 2022, 55, 8757−8765

Federico Zontone − *European Synchrotron Radiation Facility, 38043 Grenoble, France*
Luigi Cristofolini − *Department of Mathematical, Physical and Computer Sciences, University of Parma, 43124 Parma, Italy*
Christian Gutt − *Department Physik, Universität Siegen, 57072 Siegen, Germany*

Complete contact information is available at: https://pubs.acs.org/10.1021/acs.macromol.2c01326

Notes

The authors declare no competing financial interest.

■ ACKNOWLEDGMENTS

We acknowledge the provision of beamtime by ESRF and DESY for these experiments and the support from the beam line staff at ID10 and P10 during the preparation of the experiments and the beamtimes. CG acknowledges support from BMBF via projects 05K19PS1 and Röntgen-Ångström Cluster Grant 05K20PSA.

■ REFERENCES

(1) Rezazadeh, H.; Moghadam, P. N.; Ehsanimehr, S.; Fareghi, A. R. Synthesis of a New Magnetic Nanocomposite Hydrogel Based on Poly(Vinyl Acetate-Co-Maleic Anhydride)/Melamine for Efficient Dye Removal. *J. Elastomers Plastics* **2020**, *52*, 70−89.
(2) Bockstaller, M. R.; Thomas, E. L. Optical Properties of Polymer-Based Photonic Nanocomposite Materials. *J. Phys. Chem. B* **2003**, *107*, 10017−10024.
(3) Sanchez, C.; Lebeau, B.; Chaput, F.; Boilot, J.-P. Optical Properties of Functional Hybrid Organic-Inorganic Nanocomposites. *Adv. Mater.* **2003**, *15*, 1969−1994.
(4) Chen, Q.; Gong, S.; Moll, J.; Zhao, D.; Kumar, S. K.; Colby, R. H. Mechanical Reinforcement of Polymer Nanocomposites from Percolation of a Nanoparticle Network. *ACS Macro Lett.* **2015**, *4*, 398−402.
(5) Moll, J. F.; Akcora, P.; Rungta, A.; Gong, S.; Colby, R. H.; Benicewicz, B. C.; Kumar, S. K. Mechanical Reinforcement in Polymer Melts Filled with Polymer Grafted Nanoparticles. *Macromolecules* **2011**, *44*, 7473−7477.
(6) Dell, Z. E.; Schweizer, K. S. Theory of Localization and Activated Hopping of Nanoparticles in Cross-Linked Networks and Entangled Polymer Melts. *Macromolecules* **2014**, *47*, 405−414.
(7) Yamamoto, U.; Schweizer, K. S. Theory of Nanoparticle Diffusion in Unentangled and Entangled Polymer Melts. *J. Chem. Phys.* **2011**, *135*, 224902.
(8) Yamamoto, U.; Schweizer, K. S. Microscopic Theory of the Long-Time Diffusivity and Intermediate-Time Anomalous Transport of a Nanoparticle in Polymer Melts. *Macromolecules* **2015**, *48*, 152−163.
(9) Cai, L.-H.; Panyukov, S.; Rubinstein, M. Mobility of Nonsticky Nanoparticles in Polymer Liquids. *Macromolecules* **2011**, *44*, 7853−7863.
(10) Gao, W.; Zhang, Y.; Zhang, Q.; Zhang, L. Nanoparticle-Hydrogel: A Hybrid Biomaterial System for Localized Drug Delivery. *Ann. Biomed. Eng.* **2016**, *44*, 2049−2061.
(11) Cai, L.-H.; Panyukov, S.; Rubinstein, M. Hopping Diffusion of Nanoparticles in Polymer Matrices. *Macromolecules* **2015**, *48*, 847−862.
(12) Gardel, M. L.; Valentine, M. T.; Crocker, J. C.; Bausch, A. R.; Weitz, D. A.Microrheology of Entangled F-Actin Solutions. *Phys. Rev. Lett.***2003**, *91*. DOI: 10.1103/PhysRevLett.91.158302
(13) Mason, T. G.; Weitz, D. A. Optical Measurements of Frequency-Dependent Linear Viscoelastic Moduli of Complex Fluids. *Phys. Rev. Lett.* **1995**, *74*, 1250−1253.
(14) Guo, H.; Bourret, G.; Lennox, R. B.; Sutton, M.; Harden, J. L.; Leheny, R. L. Entanglement-Controlled Subdiffusion of Nanoparticles within Concentrated Polymer Solutions. *Phys. Rev. Lett.* **2012**, *109*, 055901.
(15) Cates, M. E.; Candau, S. J. Statics and Dynamics of Worm-like Surfactant Micelles. *J. Phys.: Condens. Matter* **1990**, *2*, 6869−6892.
(16) Dreiss, C. A. Wormlike Micelles: Where Do We Stand? Recent Developments, Linear Rheology and Scattering Techniques. *Soft Matter* **2007**, *3*, 956.
(17) Matsumoto, S.; Yamaguchi, S.; Ueno, S.; Komatsu, H.; Ikeda, M.; Ishizuka, K.; Iko, Y.; Tabata, K. V.; Aoki, H.; Ito, S.; Noji, H.; Hamachi, I. Photo Gel-Sol/Sol-Gel Transition and Its Patterning of a Supramolecular Hydrogel as Stimuli-Responsive Biomaterials. *Chem.—Eur. J.* **2008**, *14*, 3977−3986.
(18) Chu, Z.; Dreiss, C. A.; Feng, Y. Smart Wormlike Micelles. *Chem. Soc. Rev.* **2013**, *42*, 7174.
(19) Feng, Y.; Chu, Z.; Dreiss, C. A.Smart Wormlike Micelles. *SpringerBriefs in Molecular Science*; Springer Berlin Heidelberg: Berlin, Heidelberg, 2015.
(20) Cates, M. E. Reptation of Living Polymers: Dynamics of Entangled Polymers in the Presence of Reversible Chain-Scission Reactions. *Macromolecules* **1987**, *20*, 2289−2296.
(21) Lee, J.; Grein-Iankovski, A.; Narayanan, S.; Leheny, R. L. Nanorod Mobility within Entangled Wormlike Micelle Solutions. *Macromolecules* **2017**, *50*, 406−415.
(22) Grübel, G.; Zontone, F. Correlation Spectroscopy with Coherent X-rays. *J. Alloys Compd.* **2004**, *362*, 3−11.
(23) Gutt, C.; Stadler, L.-M.; Duri, A.; Autenrieth, T.; Leupold, O.; Chushkin, Y.; Grübel, G. Measuring Temporal Speckle Correlations at Ultrafast X-Ray Sources. *Opt. Express* **2009**, *17*, 55.
(24) Leheny, R. L. XPCS: Nanoscale Motion and Rheology. *Curr. Opin. Colloid Interface Sci.* **2012**, *17*, 3−12.
(25) Madsen, A.; Fluerasu, A.; Ruta, B.Structural Dynamics of Materials Probed by X-Ray Photon Correlation Spectroscopy. In *Synchrotron Light Sources and Free-Electron Lasers*; Jaeschke, E., Khan, S., Schneider, J. R., Hastings, J. B., Eds.; Springer International Publishing: Cham, 2015; pp 1−21.
(26) Ketner, A. M.; Kumar, R.; Davies, T. S.; Elder, P. W.; Raghavan, S. R. A Simple Class of Photorheological Fluids: Surfactant Solutions with Viscosity Tunable by Light. *J. Am. Chem. Soc.* **2007**, *129*, 1553−1559.
(27) Tao, J.; Yang, H.-y.; Hao, X.; Xie, Y.-j.; Li, H.-y. Effect of Ortho-Methoxycinnamic Acid on the Sol-Gel Transition of Methylcellulose Solutions in the Presence of Cetyltrimethylammonium Bromide. *Chin. J. Polym. Sci.* **2013**, *31*, 263−274.
(28) Cohen, M. D. The Photochemistry of Organic Solids. *Angew. Chem., Int. Ed. Engl.* **1975**, *14*, 386−393.
(29) Atkinson, S. D. M.; Almond, M. J.; Hibble, S. J.; Hollins, P.; Jenkins, S. L.; Tobin, M. J.; Wiltshire, K. S. An in Situ Time-Dependent Study of the Photodimerisation of Chloro-Derivatives of Trans-Cinnamic Acid Using Infrared Microspectroscopy with a Synchrotron Radiation Source. *Phys. Chem. Chem. Phys.* **2004**, *6*, 4.
(30) Chen, W.-R.; Butler, P. D.; Magid, L. J. Incorporating Intermicellar Interactions in the Fitting of SANS Data from Cationic Wormlike Micelles. *Langmuir* **2006**, *22*, 6539−6548.
(31) Kern, F.; Lemarechal, P.; Candau, S. J.; Cates, M. E. Rheological Properties of Semidilute and Concentrated Aqueous Solutions of Cetyltrimethylammonium Bromide in the Presence of Potassium Bromide. *Langmuir* **1992**, *8*, 437−440.
(32) Porte, G.; Gomati, R.; El Haitamy, O.; Appell, J.; Marignan, J. Morphological Transformations of the Primary Surfactant Structures in Brine-Rich Mixtures of Ternary Systems (Surfactant/Alcohol/Brine). *J. Phys. Chem.* **1986**, *90*, 5746−5751.
(33) Appell, J.; Porte, G.; Khatory, A.; Kern, F.; Candau, S. J. Static and Dynamic Properties of a Network of Wormlike Surfactant Micelles (Cetylpyridinium Chlorate in Sodium Chlorate Brine). *J. Phys.* **1992**, *2*, 1045−1052.
(34) Croce, V.; Cosgrove, T.; Maitland, G.; Hughes, T.; Karlsson, G. Rheology, Cryogenic Transmission Electron Spectroscopy, and Small-

Angle Neutron Scattering of Highly Viscoelastic Wormlike Micellar Solutions. *Langmuir* **2003**, *19*, 8536−8541.
(35) Cates, M. Dynamics of Living Polymers and Flexible Surfactant Micelles : Scaling Laws for Dilution. *J. Phys.* **1988**, *49*, 1593−1600.
(36) Bée, M.*Quasielastic Neutron Scattering: Principles and Applications in Solid State Chemistry, Biology, and Materials Science*; Adam Hilger: Bristol, England, Philadelphia, 1988; p 370.
(37) Cristofolini, L.; Facci, P.; Fontana, M. P.; Cicognani, G.; Dianoux, A. J. Lithium diffusion andC60dynamics by quasielastic and inelastic neutron scattering inLi12C60fulleride. *Phys. Rev. B: Condens. Matter Mater. Phys.* **2000**, *61*, 3404−3409.
(38) Cristofolini, L.; Dianoux, A.; Damay, P. A Particle Jumping in an Octahedron Studied by QENS. *Phys. B* **2000**, *276-278*, 316−317.
(39) May, S.; Bohbot, Y.; Ben-Shaul, A. Molecular Theory of Bending Elasticity and Branching of Cylindrical Micelles. *J. Phys. Chem. B* **1997**, *101*, 8648−8657.
(40) Sharma, A.; Licup, A. J.; Rens, R.; Vahabi, M.; Jansen, K. A.; Koenderink, G. H.; MacKintosh, F. C. Strain-Driven Criticality Underlies Nonlinear Mechanics of Fibrous Networks. *Phys. Rev. E* **2016**, *94*, 042407.
(41) Sharma, A.; Licup, A. J.; Jansen, K. A.; Rens, R.; Sheinman, M.; Koenderink, G. H.; MacKintosh, F. C. Strain-Controlled Criticality Governs the Nonlinear Mechanics of Fibre Networks. *Nat. Phys.* **2016**, *12*, 584−587.
(42) Rens, R.; Vahabi, M.; Licup, A. J.; MacKintosh, F. C.; Sharma, A. Nonlinear Mechanics of Athermal Branched Biopolymer Networks. *J. Phys. Chem. B* **2016**, *120*, 5831−5841.
(43) Pritchard, R. H.; Shery Huang, Y. Y. S.; Terentjev, E. M. Mechanics of Biological Networks: From the Cell Cytoskeleton to Connective Tissue. *Soft Matter* **2014**, *10*, 1864−1884.
(44) Jansen, K. A.; Licup, A. J.; Sharma, A.; Rens, R.; MacKintosh, F. C.; Koenderink, G. H. The Role of Network Architecture in Collagen Mechanics. *Biophys. J.* **2018**, *114*, 2665−2678.

https://doi.org/10.1021/acs.macromol.2c01326
Macromolecules 2022, 55, 8757−8765